Magnetic pinning of flux lattice in superconducting-nanomagnet hybrids

D. Perez de Lara,[1,2] F. J. Castaño,[3] B. G. Ng,[3] H. S. Körner,[3] R. K. Dumas,[4]
E. M. Gonzalez,[2] Kai Liu,[4] C. A. Ross,[3] Ivan K. Schuller,[5] and J. L. Vicent[1,2,a]

[1]*IMDEA-Nanociencia, Cantoblanco, Madrid 28049, Spain*
[2]*Departamento de Fisica de Materiales, Universidad Complutense, Madrid 28040, Spain*
[3]*Department of Materials Science and Engineering, Massachusetts Institute of Technology, Cambridge Massachusetts 02139, USA*
[4]*Physics Department, University of California, Davis, California 95616, USA*
[5]*Physics Department, University of California-San Diego, California 92093, USA*

Strong superconducting pinning effects are observed from magnetic landscapes produced by arrays of circular rings with varying magnetic remanent states. The collective and the background pinning of superconducting Nb films is strongly enhanced by the stray magnetic field produced by an array of circular Ni rings magnetized to form "onion" (bidomain) states. On the other hand, when the same rings are magnetized into vortex (flux-closed) states, or are randomly magnetized, the superconducting pinning is much smaller. The greatest pinning is produced when the superconducting vortex lattice motion is along a direction in which there is a strong magnetic field variation. © *2011 American Institute of Physics*. [doi:10.1063/1.3659292]

Vortices occur in a wide range of quantum fluids.[1,2] Due to their mutual interactions, superconducting vortices order into regular vortex lattices in defect-free materials. The structure and dynamics of the vortex lattice is significantly affected by interactions with intrinsic and extrinsic artificially prepared pinning centers. The motion of the normal cores of superconducting vortices produces dissipation. This plays a key role in superconductor properties such as flux-flow resistance, critical currents, magnetization, and magnetic susceptibility. These properties are important ingredients in superconductor based applications.

The effect of magnetic pinning centers has been investigated using a variety of techniques,[3] and the influence of magnetic domains and domain walls on various superconducting properties has been reported.[4–7] In spite of this, no clear-cut experimental evidence has emerged to prove that magnetic interaction between the superconducting vortices and magnetic pinning centers plays a determining role. We show here, by manipulating the magnetic state of a pinning array of magnetic nanorings, the magnetotransport of superconducting films can be controlled and changed substantially. Previously,[8] we studied ratchet effects in similar samples to investigate the role played by magnetic potentials with broken reflection symmetry on the vortex lattice dynamics.

In this work, we have studied the magnetism and magnetotransport of hybrid superconducting Nb thin films grown on top of square-symmetry arrays of circular magnetic Ni rings [see Figure 1(a) for dimensions]. The Ni rings were prepared by electron-beam lithography on (100) Si substrates as described elsewhere.[9] The 20 nm thick Ni film was deposited by ion-beam sputtering while the 100 nm Nb was magnetron-sputtered. Nb electrical contacts were patterned to form a 40 μm × 40 μm bridge.

The magnetic hysteresis of the rings was measured using alternating gradient force magnetometry. A similar array of Ni rings without a Nb layer was studied by atomic force microscopy [AFM, Fig. 1(a)], magnetic force microscopy [MFM, Fig. 1(b)], and magneto-optical Kerr effect (MOKE, Fig. 2) using the first-order reversal curve (FORC) method.[10] The 30 μm diameter MOKE laser beam probed approximately 10^3 rings simultaneously. Micromagnetic simulations were performed using the 2D OOMMF code[11] for individual rings (Fig. 1(c)) as well as arrays of 4 × 4 rings. The cell size was 4 nm × 4 nm with random cubic anisotropy in each cell. A circular "smooth" model ring had an edge roughness of 0–1 cells in amplitude. Additional modeling was performed for "rough" rings in with edge roughness amplitude as large as 2 cells (8 nm) introduced to model the roughness of the experimental sample.

A rotatable sample holder inside a superconducting magnet allowed application of H fields along different directions, i.e., in the plane of the sample, to establish different remanent states into the rings, and perpendicular to the sample for the magnetotransport measurements. The remanent states were prepared as follows. First, the Ni rings were saturated in a positive in-plane magnetic field, which was then lowered to a negative reversal field H_R, before its removal. The normalized remanence measured by MOKE (solid squares) and MFM (open circles) are shown in Fig. 2, as a function of H_R. For $H_R \geq -100$ Oe, the onion state was retained, characterized by a high remanence and two domain walls. For -400 Oe $\leq H_R \leq -300$ Oe, a vortex state was achieved at remanence in most of the rings, in which the flux closure leads to zero remanent magnetization. The inset of Fig. 2 shows both the major loop and a reversal curve ($H_R = -380$ Oe) that traces back through zero remanence. Finally, for $H_R < -450$ Oe, a stable reverse onion state was achieved which is characterized by its high negative remanence.

OOMMF simulations reproduced these experimental observations. The inset in Fig. 2 shows the calculated

[a]Author to whom correspondence should be addressed. Electronic mail: jlvicent@fis.ucm.es.
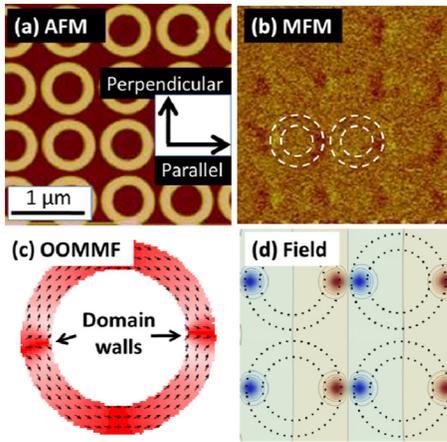
FIG. 1. (Color online) (a) AFM image of part of the sample (the ring dimensions are an outer diameter of 700 nm, a width of 125 nm, the array period is 820 nm, and covered a 100 μm × 100 μm overall area). (b) MFM images of part of the sample after being magnetized into onion states with a field from left to right. Each ring shows a black and a white contrast at the ends of a diameter corresponding to the two domain walls. Outlines of two ring locations are indicated in (b). (c) OOMMF simulation of an onion state with the 180° domain walls indicated. (d) Out-of-plane field at a height of 60 nm above the center of the rings in an onion state array, corresponding to mid-thickness of the Nb layer, calculated bases on treating the walls as monopoles. In each ring, right and left spots represent positive and negative field values.

OOMMF hysteresis loop for a single rough ring (dashed line). The onion to vortex state transition field had a strong dependence on the edge roughness, with the rough ring showing a transition field of −350 Oe compared to −50 Oe for the smooth ring. This reflected the greater pinning of magnetic domain wall motion in the rough ring. The vortex to reverse onion transition occurred near −550 Oe in both cases. The rough ring gave a closer quantitative agreement with the magnetometry data. OOMMF simulations of an array of 4 × 4 rings showed that the rings reversed over a range of fields (∼150 Oe range for the onion-vortex and ∼25 Oe range for the vortex-reverse onion transition) due to magnetostatic interactions, differences in the magnetocrystalline anisotropy, and roughness of the rings. These results showed that the majority of the rings in the array could be set into a
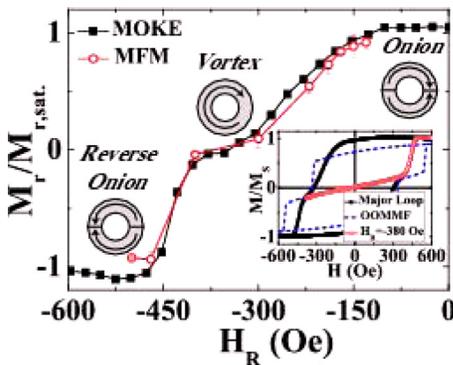
vortex state at remanence by cycling to positive saturation then to a field in the range of −300 to −400 Oe, while (reverse) onion states were produced at remanence after positive (negative) saturation.

Figure 3(a) shows the magnetoresistance of the hybrid measured at temperature $T/T_c = 0.99$, where $T_c = 8.15$ K, for the rings in different magnetic configurations, i.e., the as grown sample, in which the rings had a random distribution of remanent magnetic states, rings magnetized into flux-closed vortex states with no stray field, and rings magnetized into onion states, in this case, the superconducting vortex lattice motion parallel or perpendicular to the remanent magnetization was studied.

The number of minima and their positions are similar in all four cases, indicative of commensurability between the vortex lattice and the ring array when the vortex lattice density is an integer multiple of the density of the pinning centers. The large number of equally spaced deep minima indicates significant commensurability as compared to other
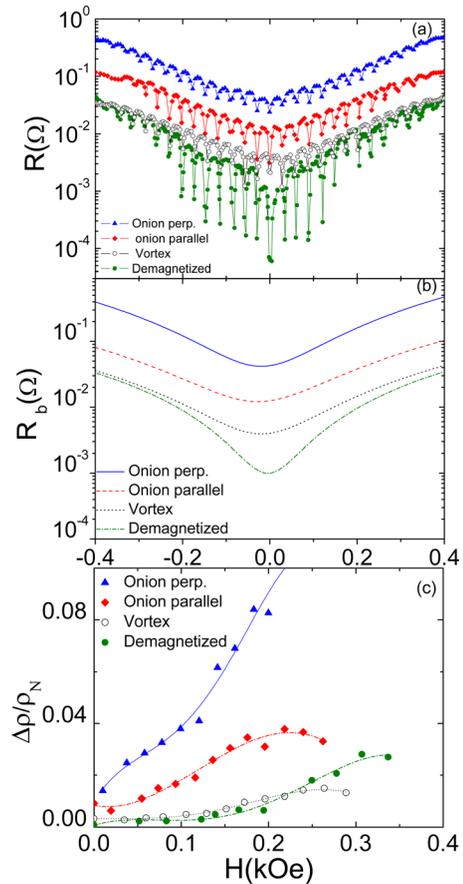

FIG. 2. (Color online) MOKE and MFM measurements of remanence after positive saturation and the subsequent application of a reverse field (H_R), with the stable remanent domain configurations indicated. The MOKE data are normalized to the remanence after saturation. The MFM data are normalized by assuming each onion state ring contributes a remanence of ±1 and each vortex state contributes 0. The inset is a major hysteresis loop measured by MOKE with a minor loop starting from −380 Oe and a calculated OOMMF hysteresis loop of a single rough circular ring.

FIG. 3. (Color online) (a) Magnetoresistance of Ni ring array covered by a Nb thin film at temperature $T = 0.99$ T/T_c. Filled green circles show data when the rings were in the demagnetized state, empty black circles from the magnetic vortex state, filled red diamonds from the onion state with vortex motion parallel to the remanent magnetization direction and blue triangles from the onion state with the vortex lattice motion perpendicular to the remanent magnetization direction. (b) Background R_b of the magnetoresistance curves of (a) fitted to a second order polynomial (green dash-dot line: demagnetized state, black dot line: magnetic vortex state, and red short dash line: onion state with the vortex motion parallel to the magnetization and blue solid line: onion state with the vortex lattice motion perpendicular to the magnetization) (c) Depth of the resistance minima normalized to the normal resistivity (ρ_N), with the same symbols as in (c) and fitted by fourth order polynomials.

geometric elements such as magnetic dots, triangles, or antidots.[3]

The field dependence of the magnetoresistance can be separated into two different contributions as shown in Figures 3(b) and 3(c). Fig. 3(b) shows the background as a function of field H obtained from a fit of the background magnetoresistance curves to a second order polynomial $R = A_0 + A_1 H + A_2 H^2$. The R-square parameters for all the polynomial regressions are above 0.97. In all the cases, the fitting coefficient ratio A_2/A_1 is of the order of 10^3, so that at $T/T_c = 0.99$, the experimentally observed flux flow resistance does not depend linearly on magnetic field but has a significant additional quadratic dependence. The (A_1, A_2) fitting parameters are greatest for the "perpendicular" measurement on the onion state and least for the demagnetized state [Fig. 3(b)]. The (A_1, A_2) parameters are temperature dependent, and the field range over which R is linear in H decreases rapidly as T/T_c increases. Therefore, the quadratic term dominates the field dependence which deviates from the linear behavior predicted by the Bardeen-Stephen theory.[12,13] This is not surprising, considering that the Bardeen-Stephen theory is valid only at zero temperatures or in the zero-magnetic-field limit at finite temperatures.

Fig. 3(c) shows the depth of the resistance minima normalized to the normal state resistivity as a function of field for the various commensuration peaks. With the rings in the onion state and the flux lattice motion perpendicular to the net magnetization, the resistance has a considerably higher background [Fig. 3(b)], stronger field dependence, and enhanced commensurability peaks. This is a clear indication of the enhanced pinning by the magnetic landscape. For motion of the vortices parallel to the remanent magnetization in the onion state, the background and peaks are smaller. The rings in the vortex state produce ideally no stray field, and the pinning in that case represents a structural effect alone.

These effects arise from the magnetic interaction between the stray fields from the 180° domain walls in the onion state at opposite ends of the ring diameter and the superconducting vortices. Fig. 1(b) indicates qualitatively the distribution of stray fields measured at a height of 65 nm for a sample without the Nb layer, with black and white contrast representing "up" and "down" fields. This scan height corresponds to a plane within the Nb layer in the Nb-coated sample. Parallel to the remanent magnetization, there is less magnetic corrugation along the direction of motion of the vortices and there are channels in the stray field distribution along which there is no magnetic corrugation at all. On the other hand, the stray fields extend over a larger distance perpendicular to the remanent magnetization, which produces an enhanced magnetic pinning landscape along the direction of vortex motion. Moreover, channeling effects also play a

crucial role in vortex dynamics as reported previously.[14,15] For vortex lattice motion perpendicular to the remanent magnetization, the out-of-plane fields reduce the superconducting channel width along the vortex motion direction while the channels are wider for motion parallel to the magnetization. These superconducting channels constrictions can be better understood in Fig. 1(d), in which the calculated field distributions for the onion state are shown as a contour plot.

In summary, we showed that the superconducting vortex dynamics can be significantly modified by changing the stray magnetic field distribution. The tunability of the remanent state of the rings enables establishing different magnetic interactions with the superconducting vortex lattice which, therefore, modifies the collective pinning. Moreover, the fact that the magnetic interaction of the superconducting vortices with the rings in the onion state is stronger than for the other remanent states is clear evidence for a magnetic interaction between the vortex lattice and the artificial pinning sites.

[1]J. R. Abo-Shaeer, C. Raman, J. M. Vogels, and W. Ketterle, Science **292**, 476 (2001).
[2]R. Blaauwgeers, V. B. Eltsov, M. Krusius, J. J. Ruohio, R. Schanen, and G. E. Volovik, Nature **404**, 471 (2000).
[3]M. Velez, J. I. Martín, J. E. Villegas, A. Hoffmann, E. M. González, J. L. Vicent, and I. K. Schuller, J. Magn. Magn. Mat. **320**, 2547 (2008).
[4]V. Vlasko-Vlasov, U. Welp, G. Karapetrov, V. Novosad, D. Rosenmann, M. Iavarone, A. Belkin, and W. K. Kwok, Phys. Rev. B **77**, 134518 (2008).
[5]A. Y. Aladyshkin, A. V. Silhanek, W. Gillijns, and V. V. Moshchalkov, Supercond. Sci. Technol. **22**, 053001 (2009).
[6]V. Vlasko-Vlasov, U. Welp, W. Kwok, D. Rosenmann, H. Claus, A. A.Buzdin, and A. Melnikov, Phys. Rev. B **82**, 100502 (2010).
[7]A. Hoffmann, L. Fumagalli, N. Jahedi, J. C. Sautner, J. E. Pearson, G. Mihajlović, and V. Metlushko, Phys. Rev. B **77**, 060506R (2008).
[8]D. Perez de Lara, F. J. Castaño, B. G. Ng, H. S. Körner, R. K. Dumas, E. M. Gonzalez, Kai Liu, C. A. Ross, I. K. Schuller, and J. L. Vicent, Phys. Rev. B **80**, 224510 (2009).
[9]F. J. Castaño, C. A. Ross, C. Frandsen, A. Eilez, D. Gil, H. I. Smith, M. Redjdal, and F. B. Humphrey, Phys. Rev. B **67**, 184425 (2003).
[10]R. K. Dumas, C. P. Li, I. V. Roshchin, I. K. Schuller, and K. Liu, Phys. Rev. B **75**, 134405 (2007).
[11]M. Donahue and D. Porter, OOMMF User's Guide, Version 1.0, NISTIR 6376 (1999).
[12]J. Bardeen and J. M. Stephen, Phys. Rev. **140**, A1197 (1965).
[13]C. F. Hempstead and Y. B. Kim, Phys. Rev. Lett. **12**, 145 (1964).
[14]M. Velez, D. Jaque, J. I. Martin, M. I. Montero, I. K. Schuller, and J. L. Vicent, Phys. Rev. B **65**, 104511 (2002).
[15]D. Perez de Lara, M. Erekhinsky, E. M. Gonzalez, Y. J. Rosen, I. K. Schuller, and J. L. Vicent, Phys. Rev. B **83**, 174507 (2011).